Combined Effects of Mass Transfer and Inaccessible Porosity in Gasification Reactions

Evangelos A. Delikouras and Daniel D. Perlmutter
Dept. of Chemical Engineering, University of Pennsylvania, Philadelphia, PA 19104

The effect of inaccessible porosity on the rate of gasification reactions is illustrated under conditions where intraparticle and extraparticle resistances to mass transfer are significant. The mathematical model developed here is based on a mass balance for the reactant fluid in the porous particle, coupled with an appropriate structural model developed for the kinetics-controlled case (Delikouras and Perlmutter, 1991). It is demonstrated numerically that the effects of inaccessible porosity generally diminish with increased diffusional resistances. In agreement with the prior kinetics-controlled case, it is shown that the effects of inaccessible porosity are more pronounced at lower values of the structural parameter Ψ and at greater levels of the inaccessible fraction.

Introduction

Since porous solids react with fluids at internal surface area, the existence of void space that is not initially accessible to the reactant fluids can have a significant effect on the reactivity of the solid. This is because this void space becomes progressively accessible in the course of reaction, due to coalescence with accessible porosity. To emphasize the fact that this void space is only temporarily inaccessible, the term hidden porosity is used interchangeably with inaccessible or isolated porosity. An earlier article (Delikouras and Perlmutter, 1991) addressed the role of inaccessible porosity in gasification reactions under conditions where chemical kinetics controlled the overall rate. The initial population of randomly overlapping pores was conceptually partitioned into two classes: one composed of only those pores that had reactive surfaces immediately accessible to the external gas and another class of inaccessible pores. A numerical study of the effects of these structural characteristics demonstrated that serious underestimations of conversion and reaction rate can occur, if existing hidden porosity is neglected. This latter porosity is reported in some instances (Kawahata and Walker, 1962; Turkdogan et al., 1970) to be as great as 40% to 50% of the total porosity.

The work presented here extends the prior analysis to include diffusional and mass-transport effects, for which the overall reaction rate is changed because reactant gases are limited in their ability to penetrate the pore structure. In gasification reactions significant resistances to mass transfer can be either external (from the bulk stream to the surface of the particle) or intraparticle (from the surface of the particle to its interior). When intraparticle resistance is important, reactant concentration is different at each position in the particle. This in turn produces a different local reaction rate and subsequently a change in the rate of reaction surface movement. Further along these lines, the reaction-stimulated discovery of previously hidden pores creates a more accessible structure which usually translates into an enhanced diffusivity of the fluid reactants.

A number of investigators have analyzed the influences of diffusional limitations on gasification reactions. Hashimoto and Silveston (1973) studied the effect of external and internal resistances on gasification behavior, by using a population balance approach that formulated the properties of interest as moments of the pore-size distribution. Bhatia and Perlmutter (1981) developed a generalized random pore model to study fluid-solid reactions in the presence of transport resistances. In a similar study, Gavalas (1981) added the effect of particle disintegration that can occur for large porosities. In none of these earlier treatments was any attempt made to account for the existence of hidden porosity.

Models that did include hidden porosity in their conceptual framework have also been developed. Reyes and Jensen (1986) applied percolation concepts to the study of char gasification in the diffusion regime. Their approach allowed for the existence of inaccessible porosity depending on the connectivity of the medium. Zygourakis and Sandmann (1988) used a discrete structural model that simulates a pore structure on a square lattice. This approach is especially promising in that it allows one to incorporate complex pore structures and dynamic

change in a realistic way. Neither study, however, provided any specific results for the effect of hidden porosity.

Mathematical Model

The reaction of a porous solid A with a surrounding gas B is considered to yield a gaseous product P, according to the following stoichiometry:

$$A_{(s)} + bB_{(g)} \rightarrow P_{(g)} \tag{1}$$

It is assumed that the heat released from this irreversible reaction is negligible and the temperature of the solid particle remains constant during the reaction. The reaction takes place at the surface of the pores of the solid. The porous structure of the solid is represented by a population of randomly intersecting cylinders of finite length. The volume fraction of those capillaries that are accessible to the reactant fluids is denoted by ϵ_o and the volume fraction of those that are not by ζ_o.

When the rate of gasification is controlled by the intrinsic kinetics of the reaction, concentration is uniform throughout the particle. However, in cases where resistance to the transport of reactant fluids from the bulk to the interior of the particle is significant, variations in concentration from point to point arise. This affects the local rate of reaction interface movement (R), which depends on the local concentration C of the reactant gas B. For first-order kinetics (Bhatia and Perlmutter, 1983):

$$R = \frac{dh_r}{dt} = k_s C \tag{2}$$

where h_r is the length by which the reaction surface moves in the normal direction and k_s is the rate constant for surface reaction. The tacit assumption in the above equation is that local concentration C is a function of only radial position (r) in the particle, an averaged value over all elements of different curvature of the reaction surface within the local differential volume. To account for the variations of concentration in a spherical particle, a mass balance for the reactant gas B is written:

$$\frac{1}{r^2}\frac{d}{dr}\left(D_e r^2 \frac{dC}{dr}\right) = \frac{\rho(1-\epsilon_o-\zeta_o)}{bM}\frac{dX}{dt} \tag{3}$$

where M and ρ are the molecular weight and density of solid A, respectively. D_e is the diffusion coefficient of gas B at a radial position r. The righthand side of Eq. 3 represents the consumption of gas B expressed via the stoichiometry of Eq. 1 in terms of conversion X of solid A. By neglecting the transient term of concentration in the mass balance, the pseudo-steady-state assumption has been invoked: it has been assumed that the porous structure changes very slowly compared to the time it takes the concentration of gas B to reach its steady-state value. Assuming radial symmetry at the center and equality of fluxes at the surface of the particle, the boundary conditions become:

$$\frac{dC}{dr} = 0 \ @ \ r = 0 \tag{4}$$

$$D_e \frac{dC}{dr} = k_m (C_b - C) \ @ \ r = r_p \tag{5}$$

where C_b is the concentration of B in the bulk stream outside the particle, k_m the mass-transfer coefficient of B between the bulk stream and the surface of the particle, and r_p the particle radius. To calculate the local reaction rate of consumption of the solid it is assumed that locally the rate is controlled by chemical kinetics. The structural model developed for the kinetic case is solved simultaneously with the aforementioned mass balance for the entire particle. The main points of the structural model are outlined below.

In the course of reaction, the pores that are initially accessible to gas B grow against the solid. In the process, they start coalescing with pores that were initially inaccessible, rendering them accessible. The volume fraction of discovered pores is denoted by V_D. Once they become accessible, these initially inaccessible or hidden pores are assumed to start growing according to the same kinetics as the originally accessible pores, and in so doing they also contribute to the discovery of the remaining hidden pores. Letting V_E and V_G be the growth of the actual pore volume that is directly attributable to the reaction of the initially accessible and discovered pores, respectively, conversion X at any instant is (Delikouras and Perlmutter, 1991):

$$X = 1 - \exp(-V_{Ex} - V_{Gx} + V_{Dx}) \tag{6}$$

where subscript x denotes the corresponding nonoverlapping volumes according to Avrami's relationship (Avrami, 1940). The rate at which hidden pores are discovered is given by the product of the rate at which total accessible porosity grows against the solid and the fractional expectation p that such a growth will uncover a hidden pore:

$$\frac{dV_{Dx}}{dt} = p\left(\frac{dV_{Ex}}{dt} + \frac{dV_{Gx}}{dt}\right) \tag{7}$$

with initial condition:

$$V_{Dx}(t=0) = 0 \tag{8}$$

By differentiating Eq. 6 with respect to time and using Eq. 7 the local reaction rate is:

$$\frac{dX}{dt} = \exp(-V_{Ex} - V_{Gx} + V_{Dx})(1-p)\left(\frac{dV_{Ex}}{dt} + \frac{dV_{Gx}}{dt}\right) \tag{9}$$

Finally, relationships are needed for V_{Ex}, V_{Gx}. The same relationships as were developed for the kinetics limiting case apply again, but here the rate of reaction interface movement depends on local concentration. The growth of the originally accessible pores follows the analytical solution:

$$V_{Ex} = k_s C S_{Eox} t + \pi (k_s C)^2 L_{Eox} t^2 \tag{10}$$

where S_{Eox} and L_{Eox} are the starting surface area and length of the initially accessible pores, respectively. The growth of the reaction surface of the discovered pores is governed by the same equations as the growth of the originally accessible ones:

$$\frac{dV_{Gx}}{dt} = k_s C S_{Gx} \tag{11}$$

$$\frac{dS_{Gx}}{dt} = 2\pi k_s C L_{Gx} \tag{12}$$

where S_{Gx} is the internal surface area of the discovered pores and L_{Gx} is the length of the discovered pores. To calculate the length of the discovered pores, information regarding the size distribution of the hidden pores is needed. Lacking experimentally based information at this time, it was assumed that the hidden pores have qualitatively the same size distribution as the accessible pores. The length of the discovered pores is considered to be proportional to the volume of the discovered pores and is given by:

$$L_{Gx} = \frac{V_{Dx}}{\epsilon_{ox}} L_{Eox} \tag{13}$$

and the corresponding initial conditions are:

$$V_{Gx}(t=0) = S_{Gx}(t=0) = 0 \tag{14}$$

In cases where the porous structure changes with time as in gasification reactions, it is expected that the effective diffusion coefficient will vary with the extent of the reaction. One may determine the dependence of the effective diffusivity on the properties of the solid by using the following relationship (Satterfield, 1970):

$$D_e = \frac{D_v \epsilon}{\gamma} \tag{15}$$

where ϵ is the total accessible porosity, D_v is an averaged value of molecular and Knudsen diffusivity, and γ is a tortuosity factor, accounting for topological features of the structure. Total accessible porosity consists of the initially accessible porosity augmented by the growth of both the initially accessible and the hidden pores. By using the definition of conversion one obtains:

$$\epsilon = \epsilon_o + V_E + V_G = \epsilon_o + V_D + X(1 - \epsilon_o - \zeta_o) \tag{16}$$

According to the model of Wakao and Smith (1962) tortuosity is given by:

$$\gamma = \frac{1}{\epsilon} \tag{17}$$

Dimensionless form

To dedimensionalize the modeling equations the following dimensionless quantities are defined:

$$\tau = k_s C_b S_{Eox} t, \quad C^* = \frac{C}{C_b}, \quad \eta = \frac{r}{r_p},$$

$$D_e^* = \frac{D_e}{D_{eo}}, \quad \epsilon^* = \frac{\epsilon}{\epsilon_o}, \quad S_{Gx}^* = \frac{S_{Gx}}{S_{Eox}} \tag{18}$$

The mass balance inside the spherical particle gives:

$$\frac{1}{\eta^2}\frac{d}{d\eta}\left(D_e^* \eta^2 \frac{dC^*}{d\eta}\right) = \phi^2 \frac{dX}{d\tau} \tag{19}$$

along with two boundary conditions:

$$\frac{dC^*}{d\eta} = 0 \ @ \ \eta = 0 \tag{20}$$

$$D_e^* \frac{dC^*}{d\eta} = Sh(1 - C^*) \ @ \ \eta = 1 \tag{21}$$

where ϕ is a modified Thiele modulus given by:

$$\phi = r_p \sqrt{\frac{\rho k_s S_o (1 - \epsilon_o - \zeta_o)}{bMD_{eo}(1 - \epsilon_o)}} \tag{22}$$

The structural model gives:

$$\frac{dX}{d\tau} = \exp(-V_{Ex} - V_{Gx} + V_{Dx})(1 - p)\left(\frac{dV_{Ex}}{d\tau} + \frac{dV_{Gx}}{d\tau}\right) \tag{23}$$

$$\frac{dV_{Dx}}{d\tau} = p\left(\frac{dV_{Ex}}{d\tau} + \frac{dV_{Gx}}{d\tau}\right) \tag{24}$$

$$\frac{dV_{Gx}}{d\tau} = S_{Gx}^* C^* \tag{25}$$

$$\frac{dS_{Gx}^*}{d\tau} = \frac{\Psi}{2}\frac{V_{Dx}}{\epsilon_{ox}} C^* \tag{26}$$

with initial conditions:

$$X(\tau=0) = V_{Dx}(\tau=0) = V_{Gx}(\tau=0) = S_{Gx}^*(\tau=0) = 0 \tag{27}$$

The following relationships are also used:

$$\Psi = \frac{4\pi L_{Eox}}{S_{Eox}^2} \tag{28}$$

$$V_{Ex} = C^*\left(\tau + \frac{\Psi \tau^2}{4} C^*\right) \tag{29}$$

$$D_e^* = (\epsilon^*)^2 \tag{30}$$

$$\epsilon^* = 1 + \frac{V_D}{\epsilon_o} + X\left(\frac{1 - \epsilon_o - \zeta_o}{\epsilon_o}\right) \tag{31}$$

Solution procedure

The system of differential equations (Eqs. 19 and 23-26) describes the temporal evolution of the porous structure. For numerical solutions, orthogonal collocation was used to discretize the spatial derivatives in Eq. 19, producing a system of ordinary differential equations that are integrated simultaneously with Eqs. 23-26. Solution of these equations yields interior profiles of conversion in the particle. Average conversion is computed by integrating local conversion over the volume of the particle:

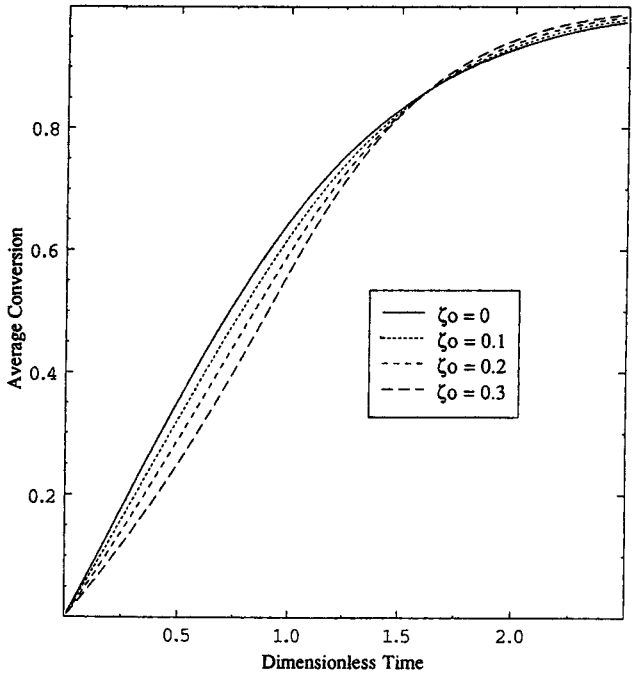

Figure 1. Average conversion as a function of time for various levels of hidden porosity ($\Psi = 1$, $\phi = 3$, $Sh = \infty$).

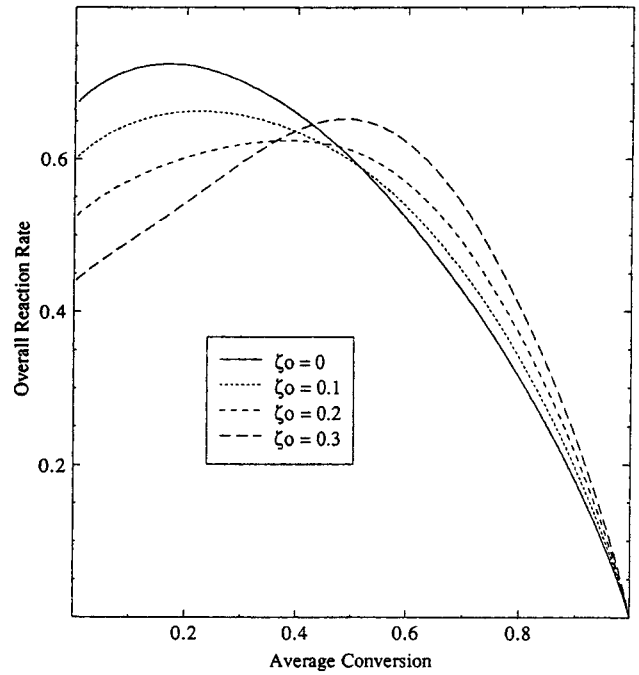

Figure 2. Gasification rate vs. conversion for various levels of hidden porosity ($\Psi = 1$, $\phi = 3$, $Sh = \infty$).

$$\hat{X} = 3 \int_0^1 X\eta^2 d\eta \tag{32}$$

and the overall rate of reaction is obtained by differentiating average conversion with respect to time. The model developed here has five parameters. The initial accessible structure of the porous medium is defined by ϵ_o and Ψ, the two measures that are sufficient to describe the gasification behavior in the kinetic regime. The Thiele modulus (ϕ) and the Sherwood number (Sh) that account for internal and external mass-transfer limitations, respectively, are needed in addition to the two structural parameters to describe the gasification behavior in the diffusion regime. Typical values for these parameters are:

$$\epsilon_o = 0.3, \quad \Psi = 1, \quad \phi = 3, \quad Sh = \infty \tag{33}$$

These values are used throughout this article, unless otherwise noted. Since they had been used before by Bhatia and Perlmutter (1981), they can also serve as a check for the model in the limiting case of a gasification reaction with no hidden porosity. The fifth parameter (ζ_o) is also structural and accounts for the initial fraction of hidden porosity.

Results and Discussion

Average conversions are presented in Figure 1 as a function of dimensionless time, for various levels of initial hidden porosity between $\zeta_o = 0$ and $\zeta_o = 0.3$. The solid line corresponds to the solution of the random pore model for no hidden porosity (Bhatia and Perlmutter, 1981) and serves as a reference for comparison. The qualitative features of the conversion curve are similar to those found in the kinetics limited case; that is, conversion is overestimated initially, because it fails to account for the volume of the discovered pores that is not converted. Deviations increase with increasing values of initial hidden porosity. Maximum deviations observed in the conversion scale are 3.3%, 7%, and 11.3% for $\zeta_o = 0.1$, 0.2, and 0.3, respectively. The corresponding relative errors are 7.5%, 17.6%, and 32.1%, respectively. For the same levels of hidden porosity the overall rate of conversion is displayed in Figure 2 as a function of average conversion. A maximum in rate occurs in each curve, although since $\Psi < 2$ monotonic behavior would have been found for $\zeta_o = 0$ under kinetic control. The location of the maximum rate is also shifted, moving towards higher conversions with increasing ζ_o. The magnitude of this maximum depends on the level of hidden porosity.

A more complete picture of this situation inside the particle is given in Figures 3 and 4. In the kinetics limiting case, concentration and conversion are uniform throughout the particle and equal to their values at the external surface of the particle, but when resistance to intraparticle diffusion is significant, a concentration and thus a conversion profile are formed. The dashed lines are the model predictions in the absence of hidden porosity ($\zeta_o = 0$), while the solid lines represent the predictions for $\zeta_o = 0.2$.

Figure 3 shows the temporal evolution of the concentration profile inside the particle, for the case of no external mass-transfer resistance (infinite Sherwood number). As time goes on, concentrations increase as expected in a gasification reaction, because mass transfer of the reactant gases is facilitated by the opening of the porous structure. Eventually, the concentration profile flattens out and approaches the concentration of the gas in the bulk stream outside the particle. This behavior is expected regardless of the existence of hidden porosity; however, concentrations in the presence of hidden porosity are consistently higher than in its absence. The

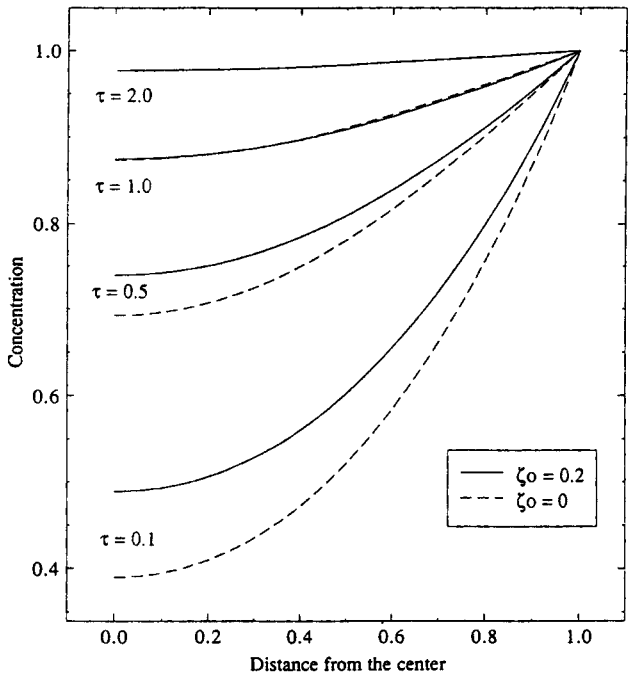

Figure 3. Concentration as a function of position inside the particle, at various times ($\Psi = 1$, $\phi = 3$, $Sh = \infty$).

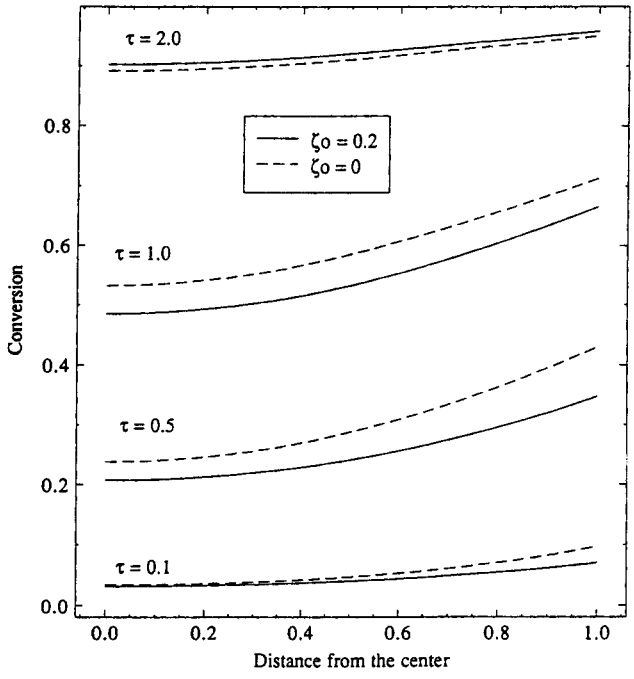

Figure 4. Conversion as a function of position inside the particle, at various times ($\Psi = 1$, $\phi = 3$, $Sh = \infty$).

explanation is that discovery of hidden pores results in a more open structure and correspondingly to a greater diffusion coefficient, according to Eq. 30. For the same reason, concentration differences increase with distance from the external surface of the particle. The effect of hidden porosity diminishes with time and eventually disappears, because its contribution to the accessible network comes to an end when all hidden porosity gets discovered.

Local conversion at various times is shown as a function of position in Figure 4. In agreement with the earlier observations, the local conversion initially lags behind the result found for no hidden porosity, but catches up and eventually surpasses it. This pattern of temporal evolution is consistent with expectation, since the discovery of hidden pores does not necessarily immediately translate into conversion. On the other hand, conversion decreases from the surface to the center of the particle because concentration follows the same pattern.

Effect of structural parameter Ψ

The effect of the structural parameter Ψ on gasification behavior is examined in Figures 5 and 6. As previously, the dashed lines represent the model predictions without hidden porosity and the solid lines are computed for $\zeta_o = 0.2$. Figure 5 shows that a larger value of Ψ imposes a faster conversion, as also observed earlier in the kinetic regime, where the structural parameter Ψ sufficed to fully describe the conversion behavior. The effect of hidden porosity is also demonstrated in the same figure, where the effect of hidden porosity decreases with increasing Ψ. In the burnoff profile (Figure 6) a shift in the position of the maximum may also be noted. The magnitude of the maximum is larger for $\Psi = 5$ and 25, but smaller for $\Psi = 1$. It is noticed that all three solid rate curves start from the same point. This is also true for the dashed lines and it can be explained by the fact that the initial rate depends only on the initial amount of hidden porosity through probability p.

Effect of intraparticle resistance

To determine the effect of the intraparticle resistance, conversion and reaction rate profiles were studied by varying the

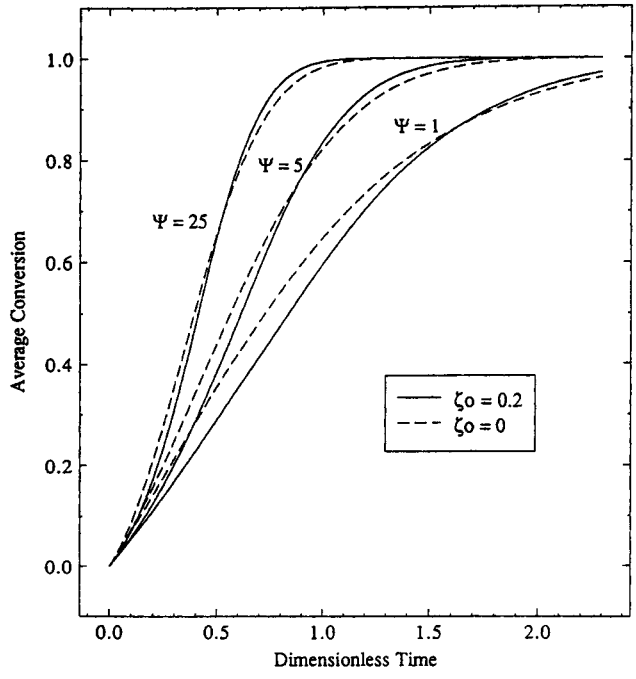

Figure 5. Effect of structural parameter Ψ on average conversion as a function of time ($\phi = 3$, $Sh = \infty$).

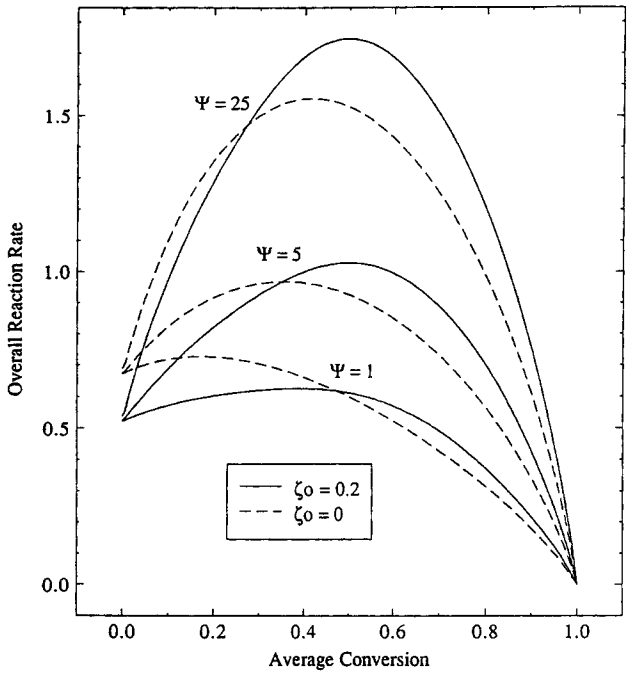

Figure 6. Burn-off profiles for various values of the structural parameter Ψ ($\phi = 3$, $Sh = \infty$).

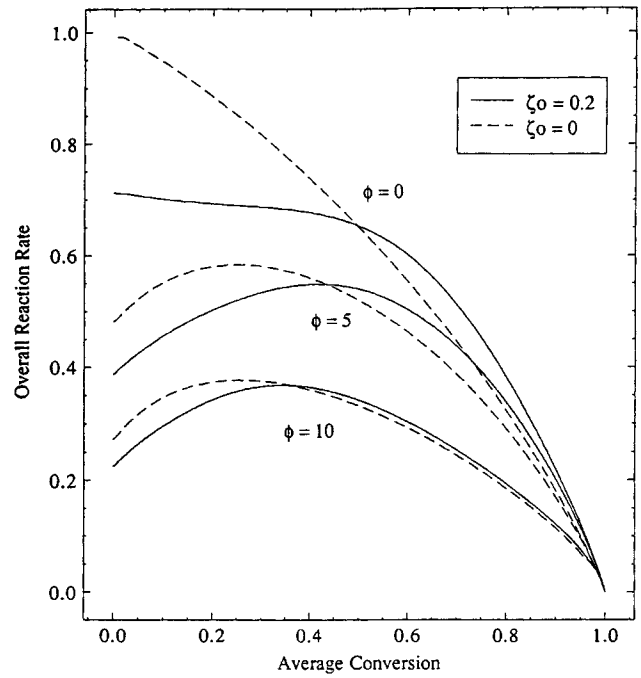

Figure 8. Burn-off profiles for various levels of Thiele modulus (Ψ = 1, $Sh = \infty$).

Thiele modulus (ϕ), a measure of the relative importance of intraparticle diffusion to chemical kinetics. In Figure 7, the line for $\phi = 0$ corresponds to the kinetically controlled case. Strong diffusional resistances begin to emerge for values of about $\phi = 10$. This regime limits the reaction of a solid to its external surface, thus forcing it to react in a shrinking core fashion. It should be noted that the model developed here may not be applicable under strong diffusional limitations, because it does not account for the change of particle radius with the extent of reaction. The conversion profile becomes steeper for lower values of Thiele modulus, because resistance to intraparticle diffusion shifts conversion closer to the surface of the particle and tends to delay gasification. In the same graph, it can be seen that the influence of hidden porosity becomes more pronounced with decreasing Thiele modulus.

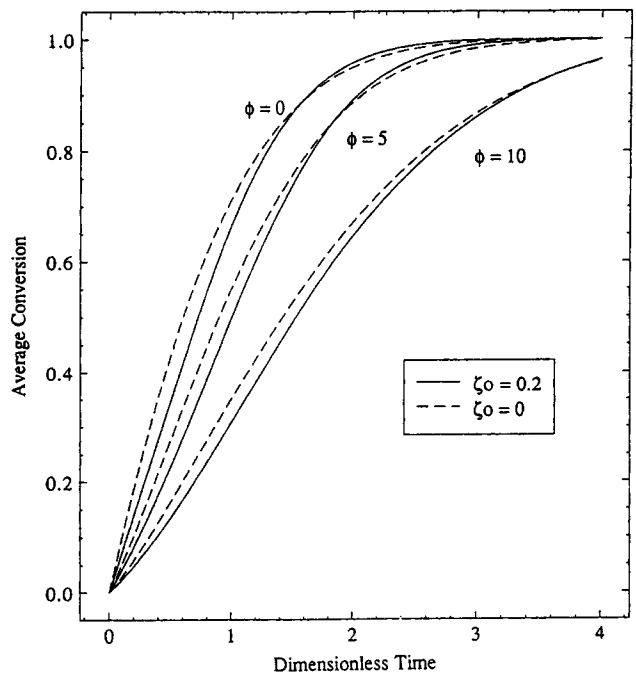

Figure 7. Effect of Thiele modulus on average conversion as a function of time (Ψ = 1, $Sh = \infty$).

The corresponding burnoff profiles are shown in Figure 8. There is no maximum in the kinetic regime, because $\Psi < 2$. In the diffusion controlled regime, maxima do occur and are shifted to higher conversions. The magnitude of those maxima is smaller compared to the maxima for no hidden porosity; however, this was not found to be universally true; for higher Ψ values the magnitude of these maxima is much larger than for the $\zeta_o = 0$ case. Differences diminish with increasing ϕ, in agreement with what was observed in Figure 7.

Effect of external resistance

The dependence of the average conversion on the magnitude of the external resistance to mass transfer is demonstrated in Figure 9, where conversion is plotted as function of time for various Sherwood numbers ($Sh = 2, 5, \infty$). Since the Sherwood number is a measure of the relative importance of internal to external mass-transfer resistances, conversion increases with increasing Sh: the lower the resistance to mass transfer, the faster the solid gasifies. The effects of hidden porosity increase with increasing Sh.

Additional interesting features arise in the burnoff profiles shown in Figure 10. The existence of hidden porosity causes significant displacement of the rate maximum; it produces more shallow rate curves at low conversions than those obtained in the absence of hidden porosity (dashed lines). The

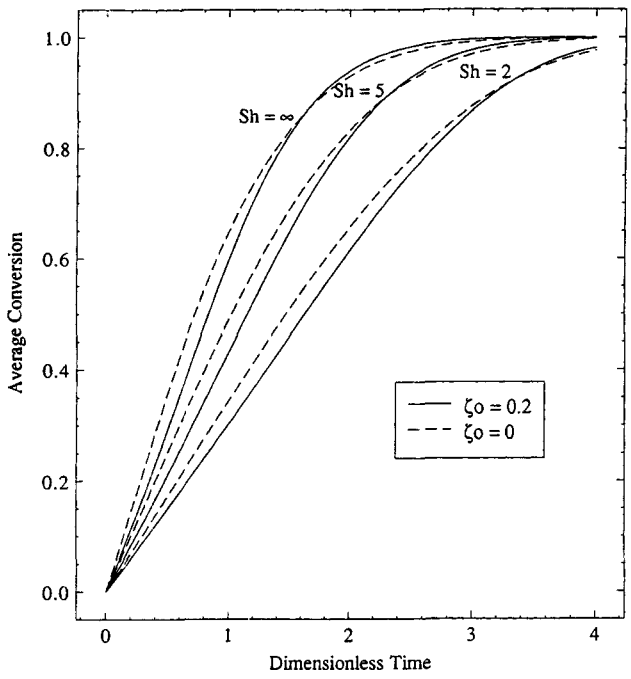

Figure 9. Effect of Sherwood number on average conversion as a function of time ($\Psi = 1$, $\phi = 3$).

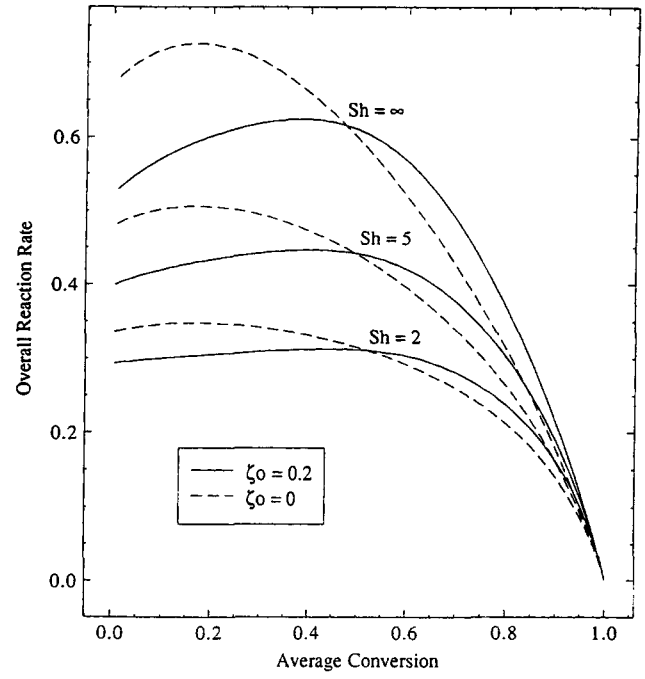

Figure 10. Burn-off profiles for various Sherwood numbers ($\Psi = 1$, $\phi = 3$).

flatness of the curves increases, while the magnitude of the rate maximum decreases with decreasing Sherwood number. These last observations are true both in the presence and in the absence of hidden porosity.

Model application

In order to provide comparisons of model predictions and experimental data, one would need to know *a priori* the amount of hidden pores in a porous particle. Unfortunately, such information is generally not available, because it is assumed that the solid skeleton of the particle is nonporous. In elaborating this point, it is not that the needed information is unattainable in principle, merely that it has not been generally measured, perhaps because the need was not as clear as it is now. A way to determine hidden porosity is by difference estimates among true solid volume, accessible pore volume and bulk volume. Accessible pore volume can be measured by mercury porosimetry or nitrogen adsorption. The true volume of the solid, also referred to as skeletal volume, can be measured by X-ray diffractometry, and bulk volume can be determined by pycnometry. Since no complete application of the model is possible where no information on the initial volume fraction of the hidden pores exists, the results given here of a parametric investigation of the magnitude of error associated with ignoring hidden porosity provide a warning against the possible effects of such porosity on gasification behavior.

Conclusions

A detailed analysis was conducted of the effects of hidden porosity on the reactivity of gasifying solids, under conditions where intraparticle and external mass transport limitations are significant. Under constant diffusional resistances, deviations from predictions which neglect hidden porosity grow bigger with increasing levels of hidden porosity and decreasing values of the structural parameter Ψ, as for the kinetics-controlled case. The selective effects of hidden porosity generally diminish when resistance to intraparticle and extraparticle diffusion increases. As a consequence, the experimental effects of hidden porosity are expected to be diluted under conditions where diffusional limitations are significant.

In comparison with earlier random pore models, the model developed here requires only one additional structural parameter: the initial fraction of the total particle volume that is inaccessible to reacting fluids. This hidden porosity can be determined experimentally from the difference between bulk volume and the sum of pore volume and skeletal solid volume. The model has as limiting cases the results of Delikouras and Perlmutter (1991) for $\phi = 0$ and those of Bhatia and Perlmutter (1981) for $\zeta_o = 0$.

Acknowledgment

The authors are indebted to Dr. S. Zarkanitis for his valuable suggestions on the numerical part of this work.

Notation

b = stoichiometric coefficient (moles of fluid B reacting with one mole of solid A)
C = local concentration of fluid B inside the porous particle
C_b = concentration of fluid B in the bulk stream outside the porous particle
D_e = effective diffusion coefficient of fluid B
D_e^* = dimensionless effective diffusion coefficient $= D_e/D_{eo}$
k_m = external boundary layer mass-transfer coefficient
k_s = reaction rate constant
L_E = total length of initially accessible pores
L_G = total length of discovered pores

M = molecular weight of solid A
p = probability of discovering a hidden pore
r = radial position in the particle
r_p = particle radius
R = rate of movement of reaction interface
S_E = surface area of initially accessible pores
S_G = surface area of discovered pores
S_{Gx}^* = dimensionless surface area of discovered pores $= S_{Gx}/S_{Eox}$
Sh = Sherwood number $= k_m r_p/D_{eo}$
t = time
V_E = volume growth of initially accessible porosity
V_G = volume growth of discovered porosity
V_D = volume of discovered porosity
V_H = volume of hidden porosity
V_T = volume of total porosity
X = local conversion
$\hat{X}$ = average conversion

Greek letters

γ = tortuosity factor
ϵ = total accessible porosity
ϵ_o = initially accessible porosity
ζ_o = initially inaccessible or hidden or isolated porosity
η = dimensionless position $= r/r_p$
ρ = density of solid A
τ = dimensionless time $= RS_{Eox}t$
ϕ = Thiele modulus $= r_p\sqrt{\dfrac{\rho k_s S_o(1-\epsilon_o-\zeta_o)}{bMD_{eo}(1-\epsilon_o)}}$
Ψ = structural parameter of the solid $= 4\pi L_{Eox}/S_{Eox}^2$

Subscripts

x = nonoverlapped quantities
o = initial quantities

Superscripts

* = dimensionless quantities

Literature Cited

Avrami, M., "Kinetics of Phase Change: II. Transformation-Time Relations of Random Distribution of Nuclei," *J. Chem. Phys.*, **8**, 212 (1940).

Bhatia, S. K., and D. D. Perlmutter, "A Random Pore Model for Fluid-Solid Reactions: II. Diffusion and Transport Effects," *AIChE J.*, **27**, 247 (1981).

Bhatia, S. K., and D. D. Perlmutter, "Unified Treatment of Structural Effects in Fluid-Solid Reactions," *AIChE J.*, **29**, 281 (1983).

Delikouras, E. A., and D. D. Perlmutter, "Inaccessible Porosity in Gasification Reactions under Kinetic Control," *AIChE J.*, **37**, 1607 (1991).

Gavalas, G. R., "Analysis of Char Combustion Including the Effect of Pore Enlargement," *Combust. Sci. Technol.*, **24**, 197 (1981).

Hashimoto, K., and P. L. Silveston, "Gasification: II. Extension to Diffusion Control," *AIChE J.*, **19**, 268 (1973).

Kawahata, M., and P. L. Walker, Jr., "Mode of Porosity Development in Activated Anthracite," *Proc. Carbon Conf.*, **2**, 251, Pergamon Press (1962).

Reyes, S., and K. F. Jensen, "Percolation Concepts in Modelling of Gas-Solid Reactions: II. Application to Char Gasification in the Diffusion Regime," *Chem. Eng. Sci.*, **41**, 345 (1986).

Satterfield, C. N., *Mass Transfer in Heterogeneous Catalysis*, M.I.T. Press, Cambridge, MA (1970).

Turkdogan, E. T., R. G. Olson, and J. V. Vinters, "Pore Characteristics of Carbon," *Carbon*, **8**, 545 (1970).

Wakao, N., and J. M. Smith, "Diffusion in Catalyst Pellets," *Chem. Eng. Sci.*, **17**, 825 (1962).

Zygourakis, K., and C. W. Sandmann, Jr., "Discrete Structural Models and Their Application to Gas-Solid Reacting Systems," *AIChE J.*, **34**, 2030 (1988).

Manuscript received May 12, 1992, and revision received Oct. 14, 1992.